Int J Adv Manuf Technol (2016) 85:1239–1247
DOI 10.1007/s00170-015-8028-8

ORIGINAL ARTICLE

Multi-objective optimization of laser brazing with the crimping joint using ANN and NSGA-II

Youmin Rong[1] · **Qi Zhou**[1] · **Yu Huang**[1] · **Yong Chang**[1] · **Guojun Zhang**[1] · **Xinyu Shao**[1]

Received: 16 June 2015 / Accepted: 25 October 2015 / Published online: 4 November 2015
© Springer-Verlag London 2015

Abstract Laser brazing process with crimping butt is sensitive to welding parameters, and it is difficult to acquire a good quality of welding joint. To achieve good welding parameters (welding speed, wire feed rate, gap), this paper addresses the multi-objective optimization of bead profile, namely sum of left side and right side of bead geometry and subtraction between top width of bead and bottom width of bead profile. Back propagation neural network was used to predict goals with average error of 9.95 and 8.54 %; non-dominated sorting genetic algorithm was adopted to acquire a Pareto set, and verification experiments demonstrated that relative errors were controlled within 3.97 %. Meanwhile, the importance from welding parameters on goals was ranked by signal-noise ratio and interactions between each parameter. Therefore, a novel multi-objective optimization method was proved to be feasible and would be useful to guide the actual welding process of laser brazing.

Keywords Laser brazing · Bead geometry · Crimping butt · Multi-objective optimization · ANN · NSGA-II

✉ Guojun Zhang
zhanggj.hust@gmail.com; 1070395117@qq.com

[1] State Key Lab of Digital Manufacturing Equipment and Technology, School of Mechanical Science and Engineering, Huazhong University of Science and Technology, Wuhan 430074, China

1 Introduction

In fact, the welding bead geometry (WBG) is the first indication of the weld bead quality [1] and that also plays an important role in determining the mechanical properties of the weld [2]. However, it is very difficult to effectively control the forming of WBG. On the one hand, WBG is firstly decided by the fluctuation of the weld pool during the welding procedure. Rao et al. found that electromagnetic force affected by shielding gas compositions plays the most significant role in determining the behaviors of metal transfer in gas metal arc welding (GMAW) [3]. Courtois et al. developed a complete modeling of heat and fluid flow mainly considering buoyancy force, Marangoni effect, and recoil pressure [4]. On the other hand, welding parameters have key influence on WBG and are difficult to be accurately regulated. Sathiya et al. revealed that shielding gas with different components have clearly impacts on bead profile, hardness, micro-structural characterization [5]. By experimental study, Phaoniam et al. researched the formation of the weld bead and the bonding strength of narrow gap welding considering wire current, wire feeding position, laser irradiation angle, and wire feeding angle [6]. Gao et al. explained the influence from heat power and welding speed on weld appearances, microhardness, and tensile properties [7]. Obviously, it is necessary to reveal the influence from welding parameters on WBG in order to better control the WBG and hence mechanical properties.

Up to now, mathematical method is a common method in developing model between the welding parameters and WBG. Sharma et al. built a WBG mathematical model of high deposition welds by supposing reinforcement as an eccentric ellipse [8]. Prasad et al. used the gray relational analysis to optimize the WBG of pulsed current micro plasma arc weld [9]. Lin et al. optimized weld shape of GMAW using hybrid model of gray relational analysis and Taguchi method [10]. Response

surface method (RSM) was applied to research the relationship between welding process (laser power, welding speed, and wire feed rate) and bead shape in narrow gap laser welding [11], while this technique was also used to relate the identified important process parameters like welding voltage, wire feed rate, welding speed, nozzle to plate distance, and welding gun angle with bead geometry in flux cored arc welding (FCAW) [12]. Korra et al. predicted and optimized the depth of penetration of the stainless steel with gas tungsten arc welding by artificial neural networks (ANN) and simulated annealing (SA) algorithm [13]. Katherasan et al. developed the mathematical simulation model of bead profile about FCAW through ANN and particle swarm optimization (PSO) algorithm and hence tested the Vickers hardness of each joint [14]. Sathiya et al. optimized the welding parameters of GMAW by RSM and Genetic algorithm (GA) [15]. For friction welding of AISI 904 L super austenitic stainless steel, gray relational analysis and the desirability approach were applied to optimize the input parameters, and GA was applied to resolve the mathematical model and to select the optimum welding parameters [16]. Meanwhile, some new methods were also induced in building the WBG mathematical model. Minimum bead width and maximum depth of penetration were calculated by imperialist competitive algorithm after that regression equations for output goals were obtained using the least squares method [17]. Multiple bead geometry parameters of submerged arc weldment were researched using Taguchi's robust design coupled with fuzzy based desirability function [18].

It is found that many researchers have focused on the prediction and optimization of the process parameters with different welding methods while the morphology of the bead profile is selected as output objectives but that usually are separated as the independent output. However, it is seldom concentrated on laser brazing with crimping butt because the brazing process is sensitive to welding parameters and difficult to acquire a good quality of the joint [19]. Meanwhile, this article is actually our team further research on the multi-objective optimization of welding parameters of the laser brazing with crimping joint.

2 Experiment setup

2.1 Material

In order to deeply research the influence from process parameters on bead profile, the laser brazing process would be further optimized [19]. The experiment base metal is double phase galvanized steel (DP590) with the size of 300×100×0.8 mm, while the length of crimping butt is 10 mm. The filler wire is $CuSi_3$ with the diameter of 1.6 mm. Meanwhile, the acetone was applied to protect DP590 from oil pollution and oxide film disturbing.

2.2 Processing conditions

In this paper, the welding parameters include welding speed (WS, 0.8~1.6 m/min), wire feed rate (WF, 2.6~3.4 m/min), and gap (GAP, 0.0~0.8 mm), and each of them is divided into five levels with 0.2 intervals. Laser power is set 3.2 KW, and defocus length is 45 mm. Welding path is obtained via a teaching method. Therefore, the experiment is designed by the 3-factor and 5-level Taguchi method L_{25}. Taguchi experimental design matrix is shown in Table 1.

2.3 Measuring features

A typical WBG of the crimping joint of laser brazing can be summarized as the top width and bottom width of bead shape (WT and WB), and the efficient connection length of left side and right side (ELL and ELR). WT and WB is linear distance of end points of the bead width, while ELL and ELR are

Table 1 Taguchi experimental design and results

NO.	WS (m/min)	WF (m/min)	GAP (mm)	SLR (mm)	STB (mm)
1	0.8	2.6	0.0	5.91	3.51
2	0.8	2.8	0.2	4.62	2.66
3	0.8	3.0	0.4	4.16	2.81
4	0.8	3.2	0.6	5.30	3.17
5	0.8	3.4	0.8	5.36	2.55
6	1.0	2.6	0.2	4.67	0.73
7	1.0	2.8	0.4	4.49	2.75
8	1.0	3.0	0.6	4.81	3.07
9	1.0	3.2	0.8	4.48	2.64
10	1.0	3.4	0.0	4.47	2.99
11	1.2	2.6	0.4	5.26	2.85
12	1.2	2.8	0.6	4.31	2.35
13	1.2	3.0	0.8	5.96	2.64
14	1.2	3.2	0.0	3.69	2.39
15	1.2	3.4	0.2	4.14	2.53
16	1.4	2.6	0.6	2.83	1.83
17	1.4	2.8	0.8	4.13	2.32
18	1.4	3.0	0.0	3.43	2.41
19	1.4	3.2	0.2	3.52	2.29
20	1.4	3.4	0.4	3.88	2.10
21	1.6	2.6	0.8	3.64	2.15
22	1.6	2.8	0.0	3.24	2.19
23	1.6	3.0	0.2	3.363	2.19
24	1.6	3.2	0.4	3.28	2.02
25	1.6	3.4	0.6	4.46	1.55

measured through manually picking up measurement point and replacing curve by linear fitting. The measurement process is completed by CSM1 software after that the weld zone is amplified through optical microscope.

2.4 Experiment results

To study the coupling influences from welding parameters on the quality of the crimping joint in laser brazing, the sum of ELL and ELR (SLR) is defined to explain the total connection length between base metal and welding zone and supposed to reflect the joint mechanical properties. The subtraction between WT and WB (STB) is also acquired to describe the esthetics of the crimping butt. Thus, higher values of SLR and STB indicate a better mechanical properties and morphology separately. The whole experiment flow is shown in Fig. 1. The 25 groups of experiment are completed by welding frame, while each bead profile is measured through CSM1 software together with optical microscope. The experiment results are shown in Table 1.

3 Optimization methodologies

The WBG optimization of the laser brazing is a high nonlinear problem, and it is difficult to develop an explicit mathematical model. To achieve a more accurate welding parameter set attached to SLR and STB, a multi-objective optimization method is established using back propagation neural network (BPNN) and non-dominated sorting genetic algorithm (NSGA-II). Flow chart is given in Fig. 2. The whole analysis process consists of experiment stage, prediction stage, and optimization stage.

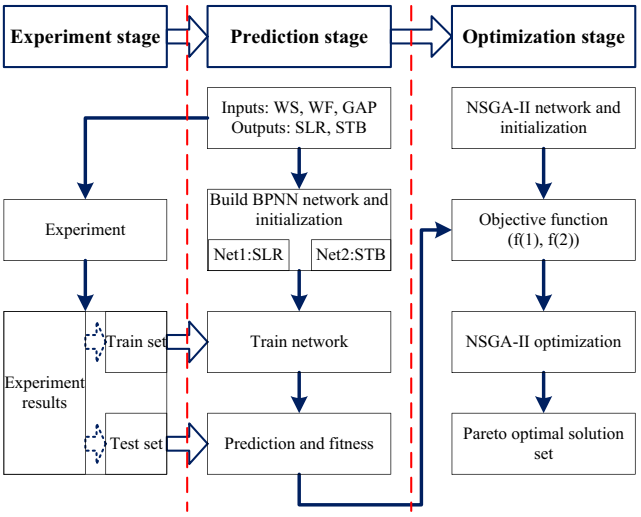

Fig. 2 Flow chart of multi-objective optimization of the crimping joint

3.1 Prediction model

In prediction stage, two networks of BPNN were developed to acquire the mathematical models in order to predict SLR and STB. As shown in Fig. 3, the net consisted of input layer (3 nodes), hidden layer (8 nodes), and output layer. The input parameters included WS, WF, and GAP, while SLR and STB were output goals. The weight between the first layer and the second layer was ω_{ij}, while ω_{jk} represented the weight from hidden layer to output layer. The fundamental concept of BPNN algorithm was the continuous improvement of the ability of the memory and learning by updating weights and thresholds according to the prediction errors. In this article, the forecasting process of bead geometry of the laser brazing with crimping butt can be summarized as the following steps.

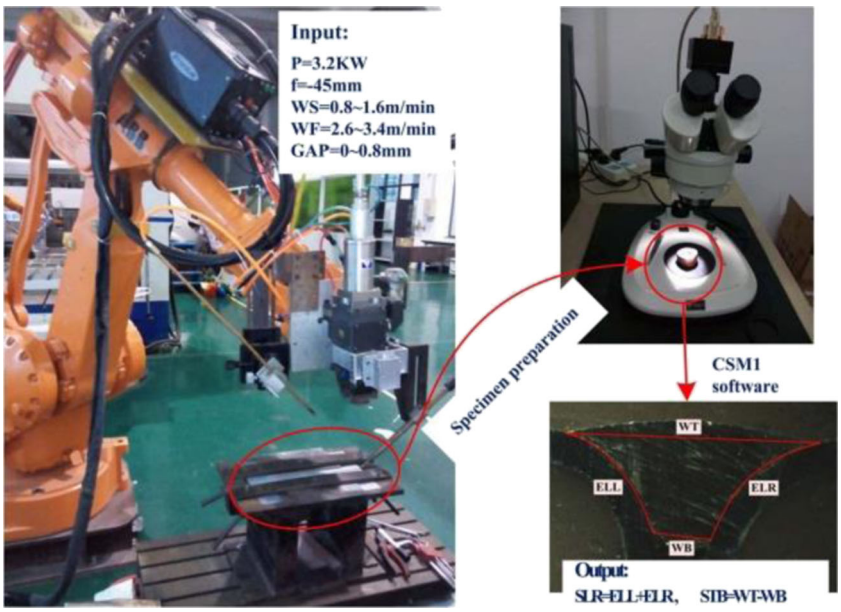

Fig. 1 Technical process of laser brazing

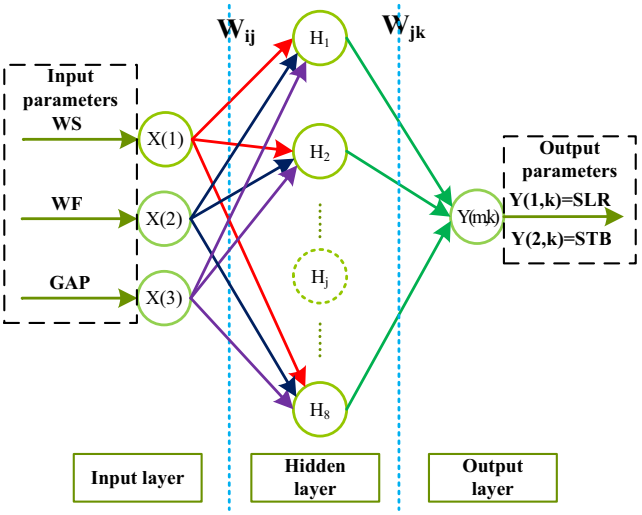

Fig. 3 Prediction networks of bead profile

Step 1: The net structural parameters, including joint weight (ω_{ij} and ω_{jk}), thresholds of the second layer and third layer (a_j and b_k), neuron excitation function (Eq. 1), are initialized after that the experiment data are divided into the train set (16 groups) and the test set (9 groups). The neuron number of the first layer ranges from 1 to 3, and that of the output layer is between 1 and 2, while the number of the hidden layer neurons keeps as 8. The maximum number of iteration is supposed as 50.

$$f(x) = \frac{1}{1+e^{x}} \tag{1}$$

where $f(x)$ is the excitation function of hidden layer and x is the input of this function.

Step 2: The results can be acquired by calculating the outputs from hidden layer (Eq. 2) and output layer (Eq. 3) in turn.

$$H(j) = f\left(\sum_{i=1}^{3} \omega_{ij}X(i) - a_j\right) \quad j = 1,2,\ldots,8 \tag{2}$$

$$Y(m,k) = \sum_{j=1}^{8} H(j)\omega_{jk} - b_k \quad m = 1 or 2, k = 1,2,\ldots,9 \tag{3}$$

where the ith input variables is represented by $X(i)$, $H(j)$ is the output of the jth neuron of the hidden layer. $Y(m,k)$ means the mth output of the kth group of the test set, while m represents the output objectives (SLR and STB).

Step 3: The prediction errors $E(m,k)$ are decided according to the difference from forecast output $Y(m,k)$ to experiment output $Y\_\exp(m,k)$ as Eq. 4.

$$E(m,k) = Y(m,k) - Y\_\exp(m,k) \tag{4}$$

Step 4: The weights (ω_{ij} and ω_{jk}) and thresholds (a_j and b_k) of the networks are refreshed based on the previous results (Eqs. 5, 6, 7, and 8). The symbol ξ represents learning rate, and its value is 0.5.

$$\omega_{ij} = \omega_{ij} + \xi H(j)\{1-[H(j)]\}X(i)\sum_{k=1}^{9} \omega_{jk}E(m,k) \tag{5}$$

$$\omega_{jk} = \omega_{jk} + \xi H(j)E(m,k) \tag{6}$$

$$a_j = a_j + \xi H(j)\{1-[H(j)]\}\sum_{k=1}^{9} \omega_{jk}E(m,k) \tag{7}$$

$$b_k = b_k + E(m,k) \tag{8}$$

Step 5: The train process would be ended and jumped to next step if the preset maximum number of iteration is reached. Otherwise, return to step 2.

Step 6: The test set is used to verify the accuracy of BPNN network.

3.2 Optimization model

As is known to all, NSGA-II considered as the out-growth of single objective algorithms has been widely used in many fields, such as vehicle design, building design, milling process, cross-docking scheduling, and so forth, while the maximum differences between NSGA-II and GA are two necessary operations (non-dominated ranking and crowding distance ranking). In this part, the multi-objective optimization model of crimping joint was developed as shown in Fig. 4. The

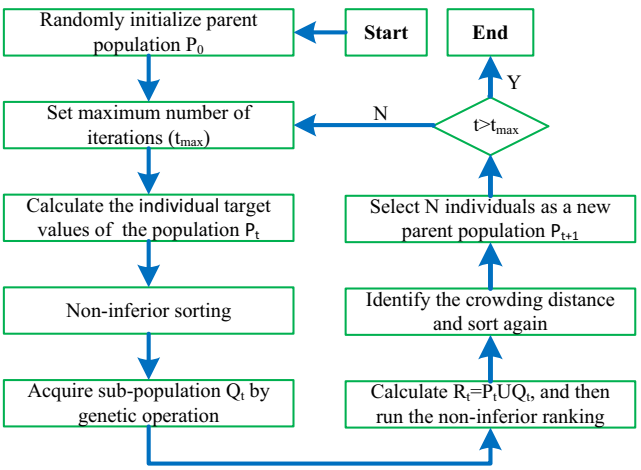

Fig. 4 Optimization process of laser brazing using NSGA-II

calculation process of NSGA-II mainly included initialization, calculation of the individual target, non-inferior sorting, identification of the crowding distance, development of a new parent population, and estimation. Meanwhile, it is necessary to explain the key steps of the NSGA-II algorithm that mainly included three aspects (initialization, non-dominance sorting, and swarm distance).

3.2.1 Initialization

The selection process of parameters of the NSGA-II model is deeply important for that it would directly decide the accuracy or even convergence of the solving procedure. Thus, the first step in Fig. 4 is random initialization of the parent population, while other structural parameters are listed in Table 2. Then, the ranges of welding parameters are extracted from Table 1. WS ranges from 0.8 to 1.6 m/min, WF is between 2.6 and 3.4 m/min, and GAP is from 0 to 0.8 mm. Meanwhile, the objective functions of SLR and STB are invoked from BPNN net1 and net2.

3.2.2 Non-dominance sorting

For dealing with multi-objective solutions, it is found that some special cases are usually similar and hence difficult to compare the superiority of these solutions with each other using dominance method. Thus, it is necessary that these cases should be ranked using a new criterion that sorts again relative to other points. The population P with number of N is divided into m subsets ($P_1, P_2, \ldots, P_m$, and $P_1 > P_2 > \ldots > P_m$), and P_{k+1} is directly dominated by the individuals in population P_k, $k=(1,2,\ldots,m)$. The sorting process of non-dominance sorting can be executed as follows:

(1) Acquire parameters (n_i and s_i) of each individual by double-loop computations
(2) Calculate the individual p_i using Eq. 9;
(3) Solve the population P_k through Eq. 10.

$$p_i = \left\{ i \middle/ n_i = 0, i \in \{1, 2, \ldots, N\} \right\} \tag{9}$$

$$P_k = \{\text{Allindividuals } i / n_i \text{ - } k + 1 = 0\} \quad k = 2, 3, \ldots, m \tag{10}$$

where each individual p_i includes two principle parameters, namely the number of individuals in the population for dominating the p_i (n_i) and the number of individuals being dominated by p_i (s_i), while the dominance relation is estimated by the values of multi-objective function.

Table 2 Parameter setting of NSGA-II algorithm

Parameter	Value
Population size	100
Maximum number of iterations	200
Deviation of fitness function	10^{-10}
Coefficient of Pareto fraction	0.3

3.2.3 Swarm distance ranking

To ensure the distribution and diversity of the solution population and acquire the uniform distribution of the fore-end of the Pareto set, the concept of swarm distance is brought in. The outstanding individual of which swarm distance is relatively short would be selected to participate in the evolution for a younger generation. Meanwhile, the swarm distance of each individual can be calculated by Eq. 11.

$$P[i]_d = \left| P[i+1]_{f_1} \text{-} P[i\text{-}1]_{f_1} \right| + \left| P[i+1]_{f_2} \text{-} P[i\text{-}1]_{f_2} \right| \tag{11}$$

where objective outputs are and f_2, $P[i]_d$ represents the swarm distance of the *ith* individual, and $P[i]_f$ is on behalf of a function value of the sub-objective f of the *ith* individual.

4 Results

4.1 Prediction results

After being built by BPNN, the prediction model was completed using MATLAB2012b. Sixteen groups of the train set (No. 1, 5, 6, 7, 8, 10, 12, 13, 15, 17, 18, 20, 22, 23, 24, 25) were randomly fed into BPNN network to acquire the accurately mathematical model, and the test set (No. 2, 3, 4, 9, 11, 14, 16, 19, 21) was used to verify the accuracy of the BPNN model. Errors (Err.) of each group of the test set can be calculated by Eq. 12, where Exp. and Pre. were abbreviation of experiment results and prediction results. The prediction results and errors were given in Fig. 5 and Table 3. The absolute values of average errors of the bead profile (SLR and STB) were respectively 9.95 and 8.54 %. The maximum error of SLR was −28.55 % and that of STB was 22.31 %. It is obvious that both average error and maximum error of SLR were all higher than that of STB. Meanwhile, this phenomenon might be caused by the

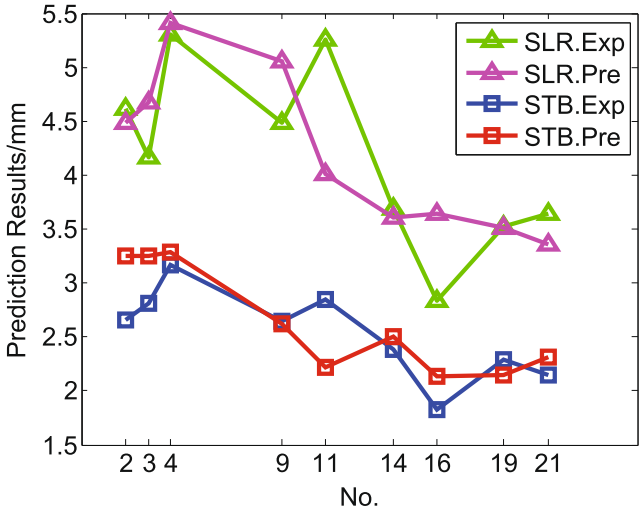

Fig. 5 Curve graph of the prediction results of the test set

experiment error and the measurement error such as the fluctuation of welding process and weld pool, assemble accuracy of galvanized steel, metering veracity of the curve of the bead shape, and so on.

$$\text{Err.} = \frac{\text{Exp.- Pre.}}{\text{Exp.}} \times 100\% \tag{12}$$

4.2 Pareto set of laser brazing with crimping butt

The multi-objective functions that would be used in optimization procedure using NSGA-II algorithm were consisted of prediction results and relevant BPNN nets. The optimization process was also realized by MATLAB2012b. Table 4 and Fig. 6 showed Pareto set with 30 groups of the laser brazing, and the distribution of Pareto set was homogeneous. The number of the Pareto set kept line with the coefficient of Pareto fraction (0.3). The values of SLR were between 3.1387 and 4.7804 mm, while that of STB ranged from 1.2837 to 1.9948 mm. The points of the Pareto set in Fig. 6 were only 29 groups because the optimization result of set No.1 was same as that of set No.11 completely.

Table 3 Prediction results of laser brazing using BPNN

No.	SLR			STB		
	Exp. (mm)	Pre. (mm)	Err. (%)	Exp. (mm)	Pre. (mm)	Err. (%)
2	4.62	4.4866	2.89	2.66	3.2452	−22.00
3	4.16	4.6717	−12.30	2.81	3.2483	−15.60
4	5.30	5.4147	−2.16	3.17	3.2812	−3.51
9	4.48	5.0527	−12.78	2.64	2.6258	0.54
11	5.26	4.0073	23.82	2.85	2.2143	22.31
14	3.69	3.6075	2.24	2.39	2.4997	−4.59
16	2.83	3.6380	−28.55	1.83	2.1336	−16.59
19	3.52	3.5162	0.11	2.29	2.1524	6.01
21	3.64	3.3632	7.60	2.15	2.3154	−7.69

Table 4 Pareto set of laser brazing with crimping butt

Set no.	WS (m/min)	WF (m/min)	GAP (mm)	f_1 (SLR, mm)	f_2 (STB, mm)
1	1.5981	3.2237	0.4435	3.1387	1.9948
2	1.5970	3.3974	0.2979	3.5532	1.8095
3	1.5973	3.3999	0.7998	4.7804	1.2837
4	1.5964	3.3981	0.3151	3.6195	1.7979
5	1.5971	3.3500	0.3301	3.3168	1.8956
6	1.5972	3.3822	0.3074	3.4619	1.8421
7	1.5925	3.3716	0.3151	3.4099	1.8636
8	1.5954	3.3966	0.3977	3.9573	1.7507
9	1.5974	3.3980	0.4445	4.1599	1.7094
10	1.5853	3.3980	0.6534	4.6529	1.5115
11	1.5981	3.2237	0.4435	3.1387	1.9948
12	1.5915	3.3977	0.6755	4.6763	1.4791
13	1.5969	3.3989	0.5791	4.5369	1.5796
14	1.5974	3.3935	0.3798	3.8507	1.7716
15	1.5936	3.3985	0.5354	4.4430	1.6299
16	1.5978	3.3968	0.3335	3.6797	1.7900
17	1.5969	3.3994	0.5089	4.3781	1.6489
18	1.5963	3.3998	0.7632	4.7560	1.3403
19	1.5897	3.3975	0.4269	4.0875	1.7304
20	1.5961	3.2704	0.3782	3.1500	1.9739
21	1.5878	3.3540	0.3493	3.3965	1.8854
22	1.5972	3.3988	0.4899	4.3201	1.6679
23	1.5978	3.3982	0.4048	4.0010	1.7386
24	1.5960	3.3993	0.6037	4.5812	1.5511
25	1.5766	3.3971	0.4721	4.2546	1.7064
26	1.5973	3.3973	0.4784	4.2743	1.6846
27	1.5926	3.3982	0.4338	4.1200	1.7206
28	1.5974	3.3977	0.3460	3.7404	1.7799
29	1.5964	3.3403	0.3376	3.2844	1.9084
30	1.5970	3.3974	0.2666	3.4735	1.8260

5 Discussion

5.1 Influence from process parameters on bead profile

For clearly revealing the complex influence from welding process on WBG and deeply explaining the reasons for some abrupt errors, it was necessary to build the concepts of signal-noise ratio (S/N) and interaction (IA) in order to demonstrate the relationship between parameters and WBG. S/N was

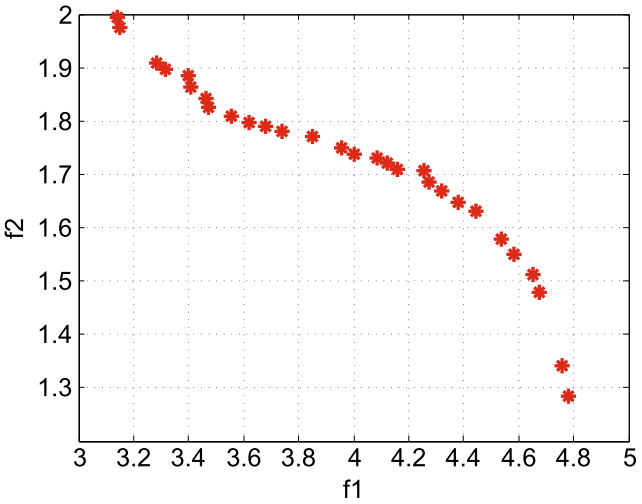

Fig. 6 Distribution of Pareto set of two objectives (f_1 and f_2)

applied to evaluate the influence from each parameter on welding quality. In other words, the extent of the impact from each welding parameter to WBG can be denoted by the value of S/N that can be calculated by Eq. 13. IA represented different effects of each level from this welding parameter to another, and the symbol of A*B was on behalf of the interaction between A (one of three welding parameters) and B (one of another two).

$$S/N = -10\log\left[\frac{1}{n}\left(\sum_{i=1}^{n}\frac{1}{Y_i^2}\right)\right] \tag{13}$$

Figure 7a showed main effects of S/N related to SLR. The S/N value of WS ranged from 10.95 to 14.04, and that of WF was between 12.02 and 12.94, while that of GAP stayed around 12.10 to 13.33. It is hence concluded that the rank of importance for SLR was WS, GAP, and WF in turn by comparing variation range of S/N values for each welding parameter. Similarly, it can be evaluated from Fig. 7b that WS had the most influence on STB while WF owned the weakest effect. As can be seen from Fig. 8, the welding parameters (WS, WF, and GAP) interacted with each other, and some IA tendencies can be summarized as follows by analyzing line graphs in Fig. 8.

For SLR,

(1) WS*WF: The WS value with level of 1.2 m/min had drastic influence on SLR, and that with 1.0 m/min owed weak effect.
(2) WS*GAP: Comparing with GAP, WS with the level of 0.8 m/min had a deeply effect on SLR, and that with 1.6 m/min owed faint influence.
(3) WF*GAP: The whole fluctuation of WF (around 2.6 m/min) on SLR was more sharply than that of other levels, and GAP had much more effects on SLR than that from WF.

For STB,

(4) WS*WF: The strong fluctuation happened on the WF-level of 2.6 m/min, and that of other four levels changed relative gently. The value of STB turned to higher with a lower WS value.
(5) WS*GAP: STB value decreased gradually with the increase of WS, while unexpected fluctuation was presented in the GAP second level of 0.2 mm.
(6) WF*GAP: The sharp fluctuation occurred in the level of 2.6 m/min of WF, while the STB values of other four levels ranged from 1.55 mm to 3.17 mm.

5.2 Verification experiment of the Pareto set

It was necessary and significant that the confirmatory experiment was carried out to demonstrate the feasibility of optimization methodology. According to the Pareto set in Table 4 and Fig. 6, one group (No.25) was randomly selected to operate verification experiment after that the welding parameters were simplified (WS 1.577 m/min, WF 3.397 m/min, GAP 0.5 mm) in order to better adapt to the actual engineering welding process, while other experiment operations were kept line with Section 2

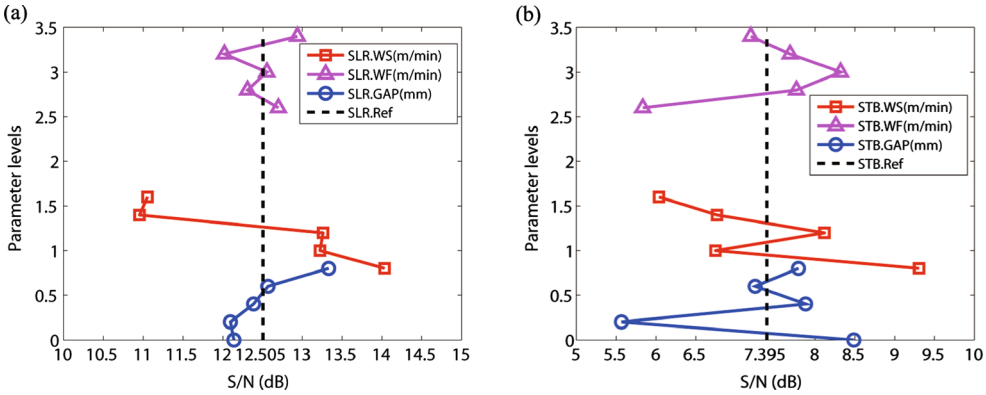

Fig. 7 Main effects of S/N of **a** SLR and **b** STB

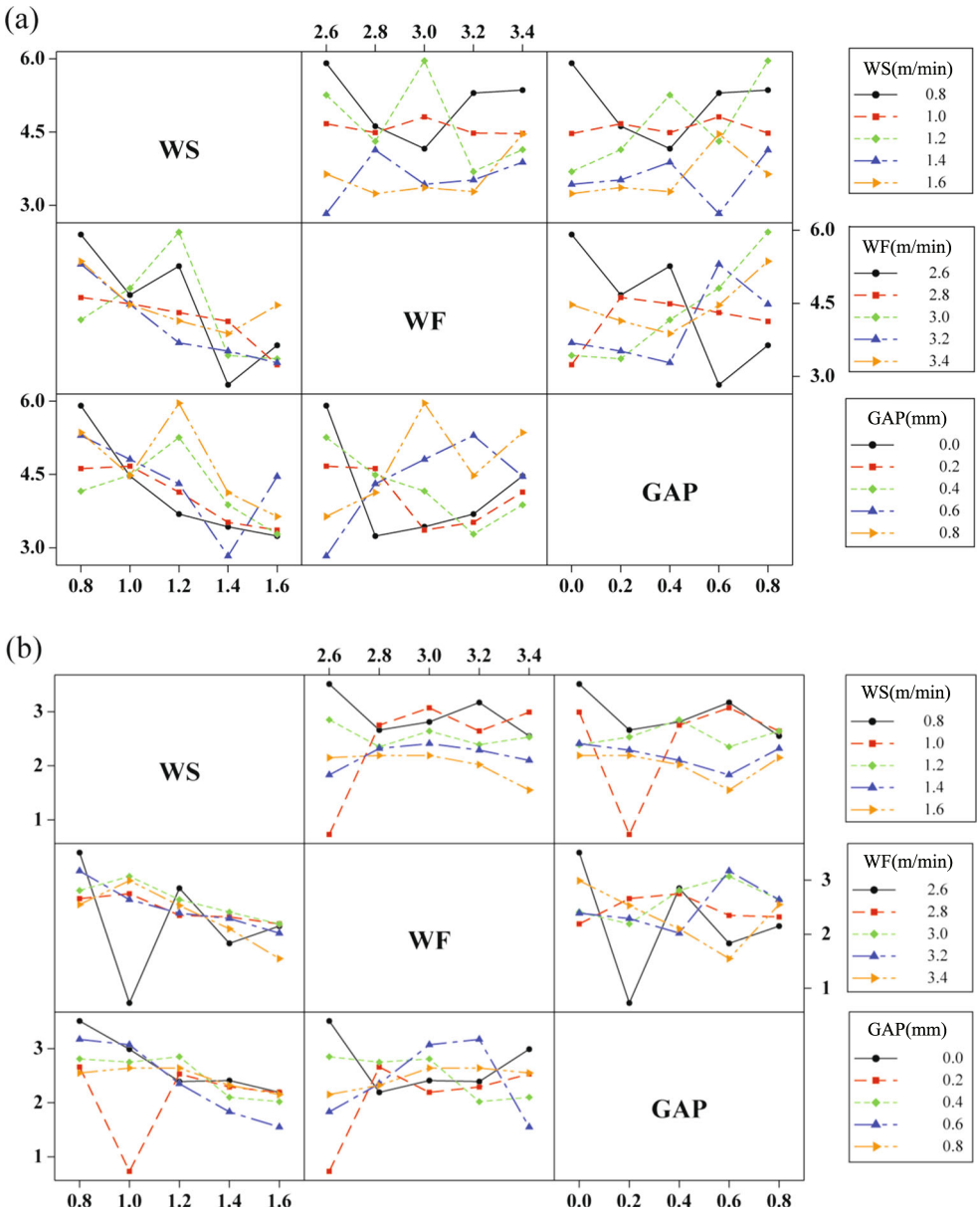

Fig. 8 Interactions between each welding parameter for **a** SLR and **b** STB

"Experiment setup". The experiment results were listed in Table 5. The errors of SLR and STB by comparing optimization result with verification experiment were 3.97 and −1.61 %. Therefore, the multi-objective optimization hybrid method using BPNN with NSGA-II together was proved to be feasible and would be useful to guide the actual welding process of laser brazing.

6 Conclusion

In this article, a further research on optimization of laser brazing with crimping joint was discussed. First two assumptions were developed: (a) SLR was applied to reflect the joint mechanical properties; (b) STB was also used to describe the esthetics of the crimping butt. Based on these assumptions,

Table 5 Results of the verification experiment

No.	ELL (mm)	ELR (mm)	WT (mm)	WB (mm)	SLR			STB		
					Exp. (mm)	Opt. (mm)	Err. (%)	Exp. (mm)	Opt. (mm)	Err. (%)
25	1.750	2.681	2.603	0.924	4.431	4.255	3.97	1.679	1.706	−1.61

prediction models of SLR and STB were built separately. Then, the Pareto set of laser brazing was acquired by NSGA-II and verified using confirmatory experiment. Meanwhile, the influence from welding process (WS, WF, and GAP) on SLR and STB was analyzed through main effects of S/N and interactions between each parameter. The following conclusions can be summarized.

(1) S/N of laser brazing process and interactions for each welding parameter on SLR and STB were analyzed, respectively, and hence, the rank of importance for SLR and STB were all WS, GAP, and WF in turn.
(2) BPNN algorithm was used to predict SLR and STB with the average error about 9.95 % and 8.54 %, and then NSGA-II was selected to acquire the Pareto set while the error of verification experiment was controlled within merely 3.97 %.
(3) The multi-objective optimization mathematical model using BPNN with NSGA-II together was proved to be feasible and would be useful to guide the actual welding process of laser brazing for crimping butt.

Acknowledgments This research are supported by the National Basic Research Program of China (973 Program, NO. 2014CB046703) and the Fundamental Research Funds for the Central Universities (HUST, NO.2014QN016). It is also very grateful to Master Longchao Cao (School of Mechanical Science and Engineering) and Master Zeyang Zhao (School of Materials Science and Engineering) for their help in experiment operations.

References

1. Aloraier A, Almazrouee A, Shehata T, Price JWH (2012) Role of welding parameters using the flux cored arc welding process of low alloy steels on bead geometry and mechanical properties. J Mater Eng Perform 21(4):540–547. doi:10.1007/s11665-011-9948-6
2. Juang SC, Tarng YS (2002) Process parameter selection for optimizing the weld pool geometry in the tungsten inert gas welding of stainless steel. J Mater Process Technol 122:33–37. doi:10.1016/S0924-0136(02)00021-3
3. Rao ZH, Hu J, Liao SM, Tsai HL (2010) Modeling of the transport phenomena in GMAW using argon–helium mixtures. Part II—the metal. Int J Heat Mass Transf 53:5722–5732. doi:10.1016/j.ijheatmasstransfer.2010.08.010
4. Courtois M, Carin M, Le Masson P, Gaied S, Balabane M (2014) A complete model of keyhole and melt pool dynamics to analyze instabilities and collapse during laser welding. J Laser Appl 26(4). doi: 10.2351/1.4886835
5. Sathiya P, Mishra MK, Soundararajan R, Shanmugarajan B (2013) Shielding gas effect on weld characteristics in arc-augmented laser welding process of super austenitic stainless steel. Opt Laser Technol 45:46–55. doi:10.1016/j.optlastec.2012.07.035
6. Phaoniam R, Shinozaki K, Yamamoto M, Kadoi K, Tsuchiya S, Nishijima A (2013) Development of a highly efficient hot wire laser hybrid process for narrow-gap welding-welding phenomena and their adequate conditions. Weld World 57:607–613. doi:10.1007/s40194-013-0055-1
7. Gao M, Tang HG, Chen XF, Zeng XY (2012) High power fiber laser arc hybrid welding of AZ31B magnesium alloy. Mater Des 42:46–54. doi:10.1016/j.matdes.2012.05.034
8. Sharma A, Arora N, Mishra BK (2015) Mathematical model of bead profile in high deposition welds. J Mater Process Technol 220:65–75. doi:10.1016/j.jmatprotec.2015.01.009
9. Prasad KS, Chalamalasetti SR, Damera NR (2015) Application of grey relational analysis for optimizing weld bead geometry parameters of pulsed current micro plasma arc welded inconel 625 sheets. Int J Adv Manuf Technol 78:625–632. doi:10.1007/s00170-014-6665-y
10. Lin HL, Yan JC (2014) Optimization of weld bead geometry in the activated GMA welding process via a grey-based Taguchi method. J Mech Sci Technol 28(8):3249–3254. doi:10.1007/s12206-014-0735-9
11. Shi H, Zhang K, Xu ZY, Huang TY, Fan LW, Bao WN (2014) Applying statistical models optimize the process of multi-pass narrow-gap laser welding with filler wire. Int J Adv Manuf Technol 75:279–291. doi:10.1007/s00170-014-6159-y
12. Senthilkumar B, Kannan T (2015) Effect of flux cored arc welding process parameters on bead geometry in super duplex stainless steel claddings. Measurement 62:127–136. doi:10.1016/j.measurement.2014.11.007
13. Sudhakaran R, Murugan VV, Sivasakthivel PS, Balaji M (2013) Prediction and optimization of depth of penetration for stainless steel gas tungsten arc welded plates using artificial neural networks and simulated annealing algorithm. Neural Comput & Applic 22:637–649. doi:10.1007/s00521-011-0720-5
14. Katherasan D, Elias JV, Sathiya P, Haq AN (2014) Simulation and parameter optimization of flux cored arc welding using artificial neural network and particle swarm optimization algorithm. J Intell Manuf 25:67–76. doi:10.1007/s10845-012-0675-0
15. Sathiya P, Ajith PM, Soundararajan R (2013) Genetic algorithm based optimization of the process parameters for gas metal arc welding of AISI 904L stainless steel. J Mech Sci Technol 27(8):2457–2465. doi:10.1007/s12206-013-0631-8
16. Balamurugan K, Mishra MK, Sathiya P, Sait AN (2014) Weldability studies and parameter optimization of AISI 904L super austenitic stainless steel Using friction welding. Mater Res-Ibero-Am J Mater 17(4):908–919. doi:10.1590/S1516-14392014005000099
17. Yazdipour A, Ghaderi MR (2014) Optimization of weld bead geometry in GTAW of CP titanium using imperialist competitive algorithm. Int J Adv Manuf Technol 72:619–625. doi:10.1007/s00170-014-5682-1
18. Singh A, Datta S, Mahapatra SS, Singha T, Majumdar G (2013) Optimization of bead geometry of submerged arc weld using fuzzy based desirability function approach. J Intell Manuf 4:35–44. doi:10.1007/s10845-011-0535-3
19. Rong YM, Zhang Z, Zhang GJ, Yue C, Gu YF, Huang Y, Wang CM, Shao XY (2015) Parameters optimization of laser brazing in crimping butt using Taguchi and BPNN-GA. Opt Lasers Eng 67:94–104. doi:10.1016/j.optlaseng.2014.10.009